FULL PAPER

Quantum Dot Based Heterostructures for Unassisted Photoelectrochemical Hydrogen Generation

Pau Rodenas, Taesup Song, Pitchaimuthu Sudhagar, Gabriela Marzari, Hyungkyu Han, Laura Badia-Bou, Sixto Gimenez,* Francisco Fabregat-Santiago, Ivan Mora-Sero, Juan Bisquert, Ungyu Paik,* and Yong Soo Kang*

TiO$_2$ hollow nanowires (HNWs) and nanoparticles (NPs) constitute promising architectures for QDs sensitized photoanodes for H$_2$ generation. We sensitize these structures with CdS/CdSe quantum dots by two different methods (chemical bath deposition, CBD and succesive ionic layer adsorption and reaction, SILAR) and evaluate the performance of these photoelectrodes. Remarkable photocurrents of 4 mA·cm and 8 mA·cm^{-2} and hydrogen generation rates of 40 ml·cm^{-2}·day^{-1} and 80 ml·cm^{-2}·day^{-1} have been obtained in a three electrode configuration with sacrificial hole scavengers (Na$_2$S and Na$_2$SO$_3$), for HNWs and NPs respectively, which is confirmed through gas analysis. More importantly, autonomous generation of H$_2$ (20 ml·cm^{-2}·day^{-1} corresponding to 2 mA·cm^{-2} photocurrent) is obtained in a two electrode configuration at short circuit under 100 mW·cm^{-2} illumination, clearly showing that these photoanodes can produce hydrogen without the assistance of any external bias. To the best of the authors' knowledge, this is the highest unbiased solar H$_2$ generation rate reported for these of QDs based heterostructures. Impedance spectroscopy measurements show similar electron density of trap states below the TiO$_2$ conduction band while the recombination resistance was higher for HNWs, consistently with the much lower surface area compared to NPs. However, the conductivity of both structures is similar, in spite of the one dimensional character of HNWs, which leaves some room for improvement of these nanowired structures. The effect of the QDs deposition method is also evaluated. Both structures show remarkable stability without any appreciable photocurrent loss after 0.5 hour of operation. The findings of this study constitute a relevant step towards the feasibility of hydrogen generation with wide bandgap semiconductors/quantum dots based heterostructures.

1. Introduction

The provision of a clean and cheap source of energy is one of the main present challenges for mankind to sustain the global social and economical development of the 21st century with minimal environmental impact. Solar energy offers a desirable alternative to the existing oil based technologies due to its inherently decentralized and inexhaustible character. Indeed, from the present catalogue of renewable energies, solar energy is the only potential candidate to fulfill the global needs, with the magnitude of the available solar power striking the earth's surface at any one instant equal to 130 million 500 MW power plants.[1]

The main factor hindering the massive exploitation of solar energy relates to its inherent seasonal and daily variability, which is asynchronous with human demand. Consequently, the storage of solar energy in chemical bonds, as nature accomplishes through photosynthesis, is one of the most promising strategies to develop a solar-based global energetic model. Following this approach, photoelectrochemical water splitting using semiconductor materials to absorb the solar radiation and convert it into H$_2$ constitutes the simplest solar to fuel conversion scheme. Since the pioneering studies of Fushijima

Dr. T. Song,[†] Dr. P. Sudhagar,[†] H. Han, L. Badia-Bou, Prof. U. Paik, Prof. Y. S. Kang
World Class University Program Department of Energy Engineering and Center for Next Generation Dye-Sensitized Solar Cells and Division of Materials Science Engineering
Hanyang University
Seoul 133-791, South Korea
E-mail: upaik@hanyang.ac.kr; kangys@hanyang.ac.kr

P. Rodenas,[†] G. Marzari, Dr. S. Gimenez, Dr. F. Fabregat-Santiago, Dr. I. Mora-Sero, Prof. J. Bisquert
Photovoltaics and Optoelectronic Devices Group
Departament de Física
Universitat Jaume I
12071 Castelló, Spain
E-mail: sjulia@fca.uji.es

[†] These authors contributed equally to this work.

and Honda on TiO_2,[2] different attempts to increase the solar-to-electricity conversion efficiency of photoelectrochemical devices have been carried out by the continuous search for new semiconductor materials and catalysts. In the recent years, the interest on this technology has significantly increased due to the advances on nanoscale design and synthesis of materials[1,3] together with the exploitation of novel optoelectronic concepts like quantum confinement,[4] band energetics engineering[5] and plasmonics.[6,7].

One of the potential strategies for efficient H_2 generation relies on harnessing the quantum confinement effects of semiconductor nanocrystals or quantum dots (QDs). Bandgap tunability by size control[4] or ligand passivation[5] allows the desired matching between the semiconductor energy levels and the formal potentials for water oxidation and hydrogen reduction. Indeed, suspended CdSe quantum dots have already demonstrated the beneficial effect of banddgap tunability for water splitting.[4] On the other hand, the sensitization of a mesoporous wide band gap semiconductor (TiO_2 or ZnO) with chalcogenide based semiconductor nanocrystals, like CdSe[8,9] CdSe/CdS[10,11] or CdTe[12] also constitutes an interesting approach for hydrogen generation in photoelectrochemical cells. In this configuration, a large surface area is provided by the mesoporous TiO_2 structure for the deposition of QDs, which also acts as a selective contact for electrons (type II junction), enhancing charge separation and minimizing electron-hole recombination. Upon supra-bandgap illumination, electron hole pairs are generated within the nanocrystals. Subsequently, holes are immediately transferred to the electrolyte and electrons are efficiently injected into TiO_2 and then transported toward the cathode by the external circuit, where the reduction of H_2 takes place. One-dimensional structures like nanowires and nanotubes constitute ideal candidates for the wide bandgap semiconductor, since they provide vectorial transport of electrons and enhanced light scattering.[13] Alternatively, ZnO/WO$_x$ hierarchical structures sensitized with CdS/CdSe quantum dots have also showed remarkable performance of 12 mA·cm^{-2} for hydrogen generation.[10] All the previous studies using this quantum dot sensitized architecture focused on the photoelectrochemical performance or gas evolution rates, without any further insight on the electronic processes leading to H_2 generation. Indeed, the chemical nature of H_2 is not always demonstrated by labeling experiments. In the present study, we carried out an integral approach focusing on the functional performance of the photoelectrodes and validated through labeling experiments. Autonomous generation of H_2 was demonstrated in a two electrode configuration at short circuit under illumination, clearly showing that the hybrid TiO_2/QDs photoanodes can produce hydrogen without the assistance of any external bias. Moreover, a detailed understanding of the electronic processes leading to H_2 generation is presented based on physical modeling fed by impedance spectroscopy characterization. This approach can also provide relevant guidelines for device optimization.
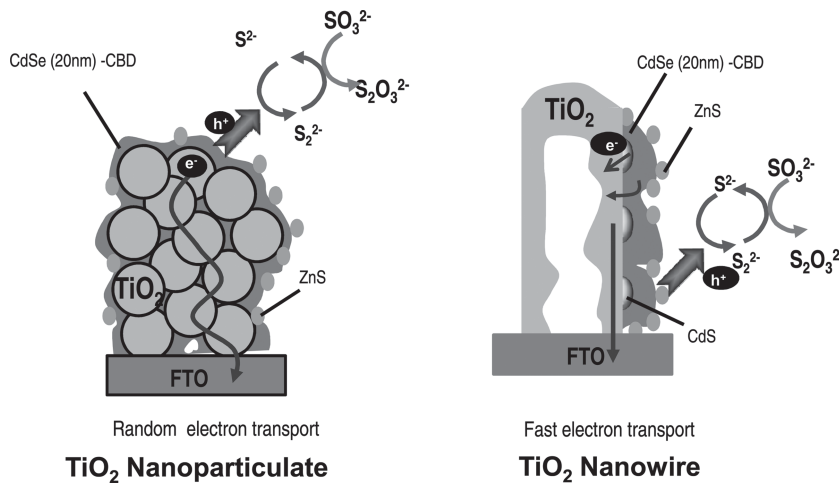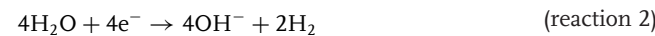

Figure 1. Oxidation at CdSe QDs-sensitized (a) TiO_2 particulate and (b) TiO_2 hollow nanowire photoanodes.

2. Results and Discussion

Figure 1 illustrates the relevant processes at the photoanode of the photoelectrochemical cell leading to hydrogen generation. When hole scavengers are present in the aqueous solution (Na_2S and Na_2SO_3), the photogenerated hole in the CdS/CdSe absorber is quickly transferred to the solution in the ps timescale[14] and the electron can be transported toward the contact. The oxidation chemistry is indicated in reaction 1. Random or vectorial electronic transport is expected for a nanoparticulated or nanowired structure respectively as showed in the cartoon. Then, the electron is driven toward the catalytic cathode by the external circuit, where the hydrogen evolution reaction takes place (reaction 2). The main reactions and steps have been discussed previously.[8,9,12,15]

$$SO_3^{2-} + S^{2-} + 2h^+ \rightarrow S_2O_3^{2-} \qquad \text{(reaction 1)}$$

$$4H_2O + 4e^- \rightarrow 4OH^- + 2H_2 \qquad \text{(reaction 2)}$$

Both hollow nanowires (HNWs) and nanoparticles (NPs) have been explored in the present study as candidate TiO_2 architectures for the development of FTO/TiO_2/CdS/CdSe heterostructures leading to hydrogen photogeneration.

Tilted high magnification SEM images of bare and CdSe deposited TiO_2 HNW arrays by CBD and SILAR methods are presented in **Figure 2**(a), Figure 2(e) and Figure 2(i), respectively. Figure 2(a) reveals that HNWs array has vertically aligned geometry and well distinct free space in between nanowires. The characteristic dimensions of this structure are: ~5 μm length (see Supplementary Information, Figure S1), ~80 nm inner radius and ~20 nm wall thickness, Figure 2(b). The surface area and porosity was estimated as 16 m^2/g and 56%, respectively (see Supplementary Information, Figure S2). The crystalline nature of HNWs was analyzed by selected area diffraction (SAED) pattern (inset of Figure 2(c)), which confirmed the polycrystalline nature of TiO_2. Lattice spacing values about 0.35 nm correspond to the d-spacing of anatase TiO_2. Figure 2(f) and Figure 2(j) provide clear information of the coverage
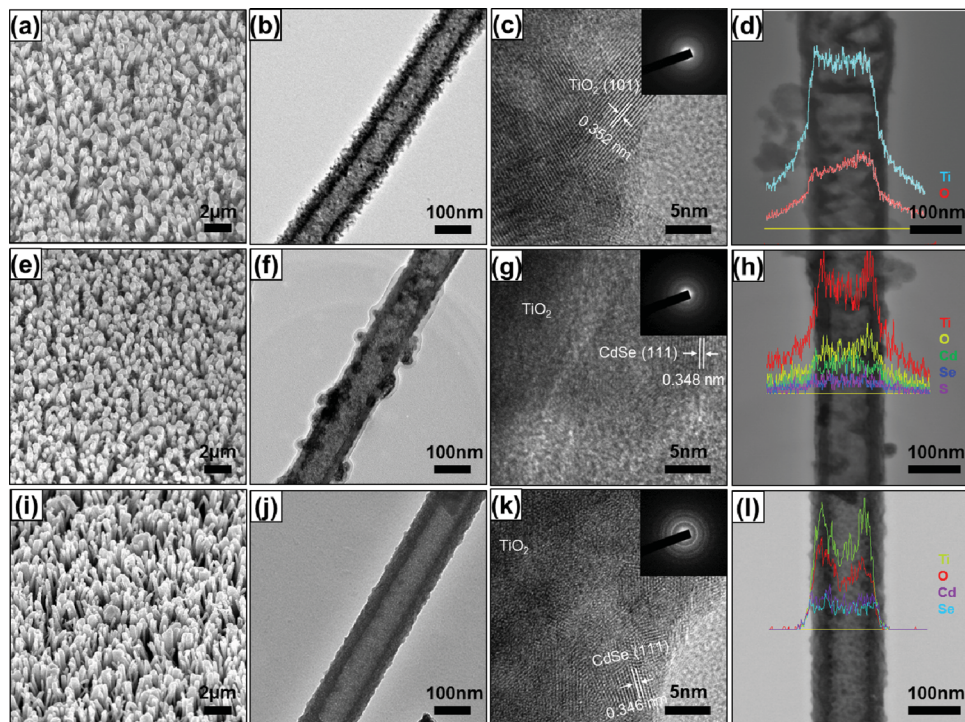
Materials
Views

www.MaterialsViews.com

ADVANCED
ENERGY
MATERIALS

www.advenergymat.de

FULL PAPER

Figure 2. SEM images of (a) pristine TiO₂ HNWs arrays, (e) TiO₂ HNWs arrays sensitized with CdSe QDs deposited by CBD and previously seeded by CdS and (i) TiO₂ HNWs arrays sensitized by SILAR deposited CdSe. High magnification TEM image of (b) pristine TiO₂ HNWs arrays at 100nm scale (f) TiO₂ HNWs arrays sensitized with CdSe QDs deposited by CBD and previously seeded by CdS and (j) TiO₂ HNWs arrays sensitized by SILAR deposited CdSe. High Resolution TEM image and selected area diffraction patterns of (c) pristine TiO₂ HNWs arrays, (g) TiO₂ HNWs arrays sensitized with CdSe QDs deposited by CBD and previously seeded by CdS and (k) TiO₂ HNWs arrays sensitized by SILAR deposited CdSe. Compositional profiles of (d) pristine TiO₂ HNWs arrays (h) TiO₂ HNWs arrays sensitized by CBD deposited CdSe and (l) TiO₂ HNWs arrays sensitized by SILAR deposited CdSe.

of CdSe on TiO_2 surface prepared by CBD and SILAR, respectively. From Figure 2(f), it is observed that ~20 nm thick CdSe nanocrystalline conformal coating on TiO_2 surface is obtained by the CBD method. In the case of SILAR deposition, decoration of CdSe nanoparticles onto the TiO_2 surface (Figure 2(j)), leads to a different film structure compared to the CBD method. The presented micrographs clearly reflect that the CBD method offers thin layer of sensitizer coverage on wide-pore structured nanowires rather than particle decoration. The crystalline structure of CdSe deposited by both CBD and SILAR techniques was further confirmed by SAED pattern evaluation and lattice d-spacing values close to 0.346 nm corresponding to (111) cubic structure were found (Figure 2(c), Figure 2(g), Figure 2(k)). The compositional line profiles Figure 2(d), Figure 2(h) and Figure 2(l) clearly confirm the CdSe sensitized TiO_2 structure without any trace of Zn and O from the nanowire growth template. An extensive structural characterization of TiO_2 NPs and TiO_2/CdS/CdSe NPs heterostructures as photoanodes for quantum dot sensitized solar cells (QDSC) has been carried out in previous studies.[16,17]

The first step in the photoelectrochemical process is the light harvesting by the sensitizer heterostructure. The optical absorbance of TiO_2 HNWs and NPs before and after CdS/CdSe sensitization is showed in **Figure 3**. Pristine TiO_2 structures can only absorb light at wavelengths below 400 nm, although the
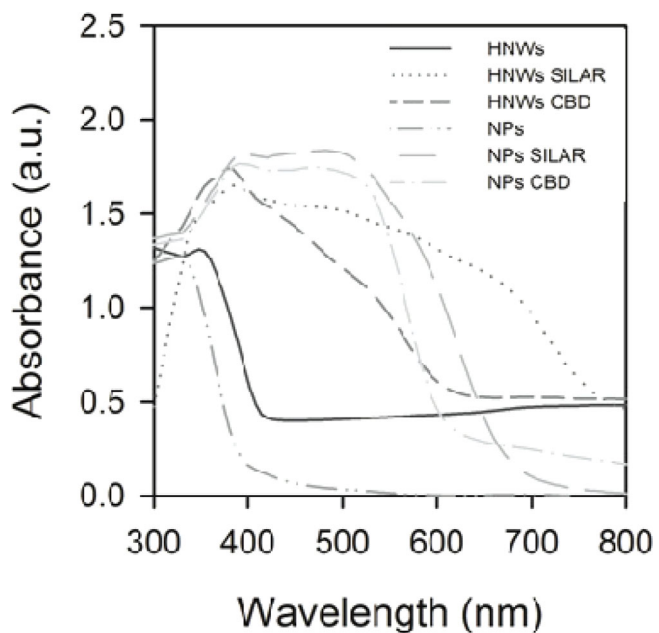

Figure 3. Absorbance calculated from transmittance and reflectance spectra for NPs and HNWs before and after CdSe sensitization by CBD and SILAR.
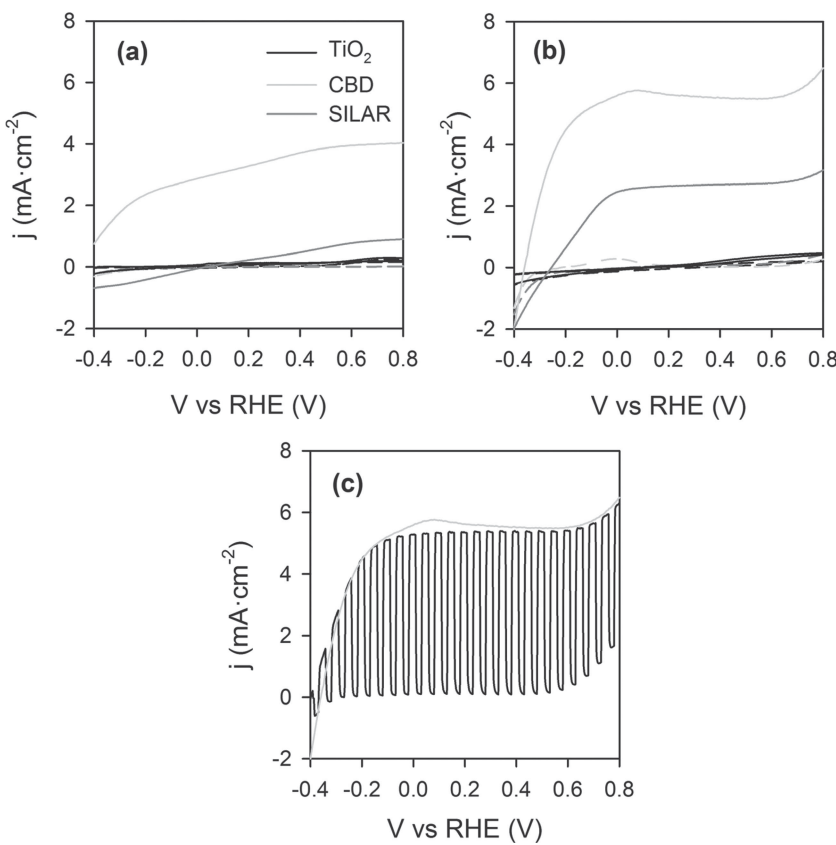
Figure 4. Current density versus potential for QDs sensitized TiO₂ photoelectrodes (a) HNWs and (b) NPs measured in dark conditions (dashed lines) and under illumination of AM 1.5 light with UV cutoff (solid lines) at 100 mW/cm², (c) a) Chopped light (black line) and steady state (grey line) j-V measured under 1 sun illumination for the NPs film with CBD QDs.

and constant light j-V curves, for TiO₂ nanoparticles sensitized by CBD. The instantaneous photocurrent density with chopped light reaches the constant light photocurrent density and remains constant until the light is turned off, where the current immediately decays to the dark value of the current, j_0. This ideal behavior is consistent with fast hole scavenging from the surface of the CdS/CdSe heterostructure to the solution.[18–20] Identical behavior has been observed for both TiO₂ architectures and both QDs deposition methods.

With the motivation of evaluating the suitability of these heterostructured photoanodes for autonomous hydrogen generation, two electrode photoeletrochemical measurements were carried out with an optimized NPs photoelectrode. The obtained result is showed in **Figure 5**(a). The maximum photocurrent was 8 mA·cm⁻² obtained at only 300 mV applied bias. More importantly, at short circuit (V = 0), 2 mA·cm⁻² (20 ml·cm⁻²·day⁻¹) are obtained under illumination, proving that these photoanodes can autonomously produce hydrogen, without the assistance of any external bias. In order to confirm that the evolved gas was hydrogen, gas chromatography and mass spectrometry experiments were carried out. From these experiments, the signature of H₂ gas in the analysed spectrum is evident, Figure 5(b). Similar results were obtained for both TiO₂ architectures. To the best of the authors knowledge, this is the highest unbiased solar H₂ generation rate reported for these QDs sensitized nanostructures.

In order to further understand the photoelectrochemical performance of the tested photoelectrodes, Impedance Spectroscopy (IS) measurements were carried out in the dark. A sound physical model for CdS/CdSe sensitized TiO₂ nanoparticulated
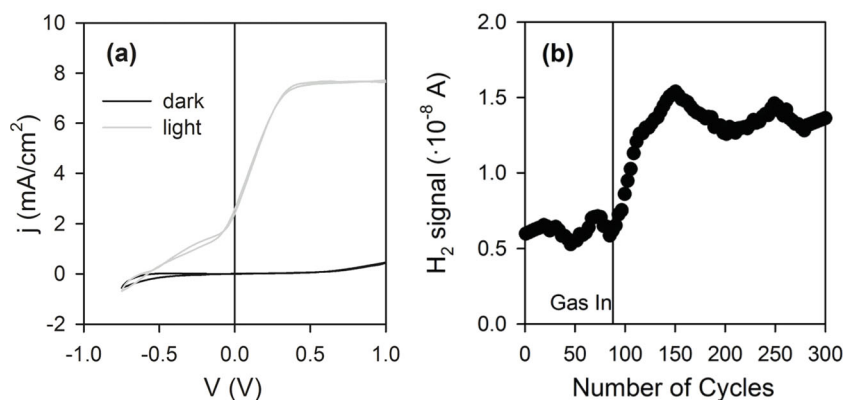
scattering of the HNWs is remarkable. After sensitization, the absorption interval of both structures extends into the visible, SILAR leading to increased absorbance compared to CBD. In any case, given the much higher surface area of NPs electrodes (73 m²/g) compared to HNWs (16 m²/g), the latter appear much more efficient light absorbers. Furthermore, the direct bandgaps for CBD and SILAR sensitized structures were calculated and the results are included as Supplementary Information, Figure S3.

The photoelectrochemical performance of both TiO₂ nanostructures for non-optimized electrodes is summarized by the steady state j-V curves of **Figure 4**(a) and Figure 4(b) in the dark and under illumination. From these figures, it is clear that the main contribution to photocurrent comes from the CdS/CdSe quantum dots, and the effect of TiO₂ on the photocurrent is marginal. Remarkable 4 mA·cm⁻² and 6 mA·cm⁻² at 100 mW·cm⁻² are obtained for HNWs and NPs respectively after CBD sensitization, which equals 40 ml·cm⁻²·day⁻¹ and 60 ml·cm⁻²·day⁻¹ hydrogen generation respectively. Figure 4(c) shows a superposition of chopped

Figure 5. (a) Current density versus potential for optimized SILAR CdS/CdSe sensitized TiO₂ NPs photoelectrodes in dark conditions and under illumination at 100 mW·cm⁻² (with UV cutoff). (b) Gas Chromatography Mass Spectroscopy plot of the evolved gas. The signal of H₂ is clearly increased after gas is passed through the system.

photoelectrodes was already developed[21,22] and we applied this model to understand the effect of the TiO_2 architecture and the QDs deposition method on the photoelectrochemical performance of the electrodes. A representative Nyquist plot for HNWs and NPs is showed in Supplementary Information, Figure S4, together with a sketch of the employed physical model. From the model fitting, we directly extracted the chemical capacitance, $C\mu$, the recombination resistance, R_{rec} and the resistivity (ρ_{TiO2}) of the TiO_2 architectures. $C\mu$ probes the electronic density of states at the Fermi level, and monitors the distribution of trap states below the conduction band, ρ_{TiO2} is the reciprocal conductivity and R_{rec} is inversely proportional to the recombination rate of electrons at the TiO_2/solution interface.[23,24] Consequently, these three parameters provide information related to the most relevant electronic mechanisms for the operation of the device. **Figure 6** shows the obtained results: the volumetric capacitance shows the expected exponential dependence with potential, reflecting the exponential tail of the density of states of TiO_2 below the conduction band. In order to obtain this calculation, the TiO_2 volume was estimated from geometrical measurements (area and thickness) and from porosity estimations from BET analysis and SEM. To compare both transport and recombination resistances between the different specimens with the same density of electrons, the chemical capacitances of all samples were shifted to make them overlap and the corrected potential is termed "equivalent conduction band potential" (V_{ecb}). This procedure has been already standarized for the evaluation of dye solar cells (DSC) and QDSC.[25] The potential shifts and the representation of the chemical capacitance versus V_{ecb} is showed in the Supplementary Information, Figure S5. In spite of the one dimensional nature of HNWs, the resistivity exhibit very similar values compared to nanoparticles (Figure 6b). This could be explained by the polycrystalline nature of the HNWs as showed in Figure 2(c), since grain boundaries are preferential sites for recombination[26] and can slow down charge transport through the material, decreasing the wire conductivity. Consequently, further optimization of these scaffold structures can be achieved for instance by doping. Indeed, N doping has demonstrated to significantly increase the performance of TiO_2 nanotubes for H_2 generation after sensitization with CdSe.[9] The recombination resistance is also generally higher for nanowires, which is expected due to the much lower surface area compared to nanoparticles (16 m²/g vs 73 m²/g), Figure 6c. This difference in surface area is also reflected in the dark j-V curves obtained by cyclic voltammetry and showed as Supplementary Information, Figure S6. The higher photocurrents systematically obtained for CBD specimens (see Figure 4) can be unambiguously ascribed to the higher recombination resistance obtained for these specimens, compared to the SILAR counterparts. This behavior can be explained on the basis of the morphological nature of the QDs deposited by both techniques, as detailed in Figure 2. CBD provides more continuous films while SILAR leads to more particle-decorated structures. Hence, recombination of electrons in the TiO_2 with holes in the electrolyte (R_{rec}) becomes more favored for heterostructures based on SILAR QDs. The shape of R_{rec} does not exhibit an exponential dependence with potential, as it should be expected, due to the exponential dependence of both $C\mu$ and R_{tr}. This behavior has also been experimentally observed in
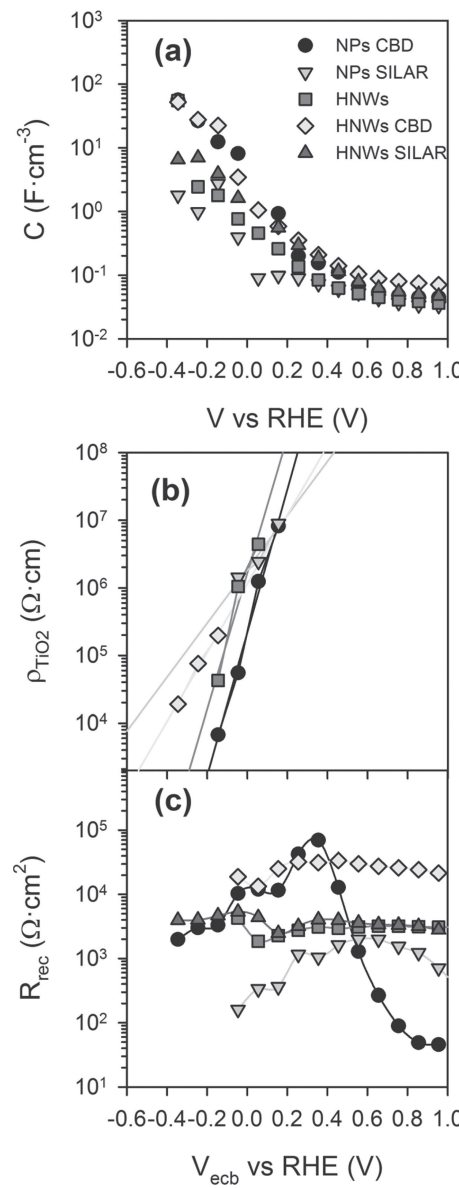

Figure 6. Parameters extracted after fitting the impedance spectroscopy spectra of HNWs and NPs sensitized by CBD and SILAR, using the model previously developed. (a) Chemical capacitance ($C\mu$), (b) TiO_2 resistivity (ρ_{TiO2}) and (c) recombination resistance (R_{rec}) as a function of potential (a), and versus the equivalent conduction band potential (V_{ecb}) (b and c). All impedance measurements were carried out in the dark. The lines in (b) are linear fittings of the experimental data. In (c) lines are drawn as eyeguides.

pristine TiO_2 nanoparticles and was ascribed to the presence of surface states.[27] An additional proof for the effect of the QDs deposition method on the recombination resistance is derived from the electron lifetime (τ_n) calculated from both IS measurements and from open-circuit voltage (V_{oc}) decay measurements for a HNWs photoelectrode (Figure S7).[28–30] Lifetimes calculated by both methods are consistent and systematically longer for CBD specimens. The difference between them can be ascribed to the active role of QDs under illumination in the recombination process.[22] Additionally, similar results were found for both TiO_2 architectures.
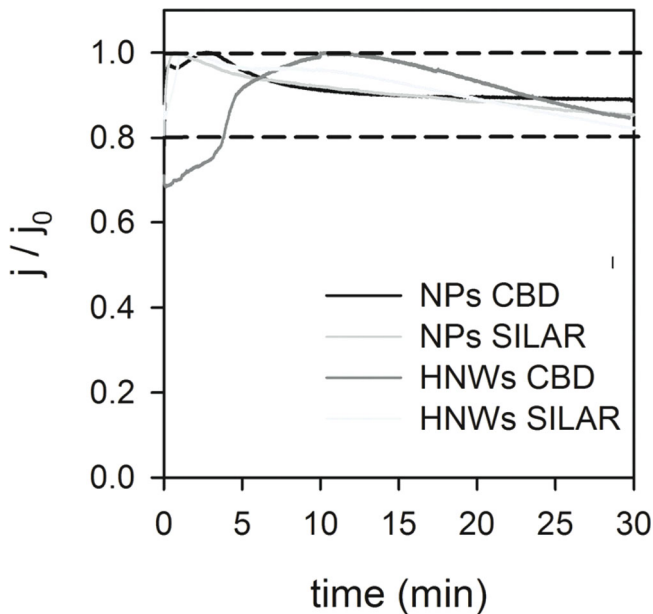
FULL PAPER

Figure 7. Chronoamperometric test for the different TiO_2-CdS/CdSe heterostructures studied, at 100 mW·cm^{-2} illumination showing the evolution of the normalized photocurrent (j/j$_0$) over time.

Finally, the stability of the device was tested by chronoamperometric measurements. Upon sample illumination at 100 mW·cm^{-2}, the short-circuit current (J$_{sc}$) was monitored over time and as showed in **Figure 7**, the photoelectrode performance was not reduced more than 10% after 30 min operation for NPs electrodes and 15% for HNWs electrodes independently of the QDs deposition method. Indeed, the observed decrease of the photocurrent was due to the consumption of the sacrificial hole scavenger and after replacing the used electrolyte for a fresh one, the performance of the photoelectrode was better compared to the initial one (Figure S8).

3. Summary and Conclusions

TiO_2 HNWs and NPs have demonstrated to be promising structures for hydrogen generation upon sensitization with CdS/CdSe QDs. CBD deposition systematically led to higher photocurrents for hydrogen generation (4 mA·cm^{-2} and 8 mA·cm^{-2} for nanowires and nanoparticles respectively, equal to 40 ml·cm^{-2}·day^{-1} and 80 ml·cm^{-2}·day^{-1} H$_2$ generation). Hydrogen generation was confirmed through gas chromatography and mass spectrometry measurements. Moreover, these electrodes produce hydrogen autonomously (2 mA·cm^{-2} or 20 ml·cm^{-2}·day^{-1} at short circuit conditions in a two electrodes cell) without the assistance of any external bias. Indeed, to the best of the author's knowledge, this is the highest autonomous solar H$_2$ generation reported for these QDs based heterostructures. By impedance spectroscopy and physical modeling, we identified the chemical capacitance of both NPs and HNWs following an exponential dependence with potential, reflecting the electron density of trap states below the TiO_2 conduction band. Similar conductivities were extracted for nanowires and nanoparticles, in spite of the vectorial transport expected for

nanowires. This could be explained by the polycrystalline nature of the nanowires and further optimization of these structures is under progress in our labs. The recombination resistance was systematically higher for nanowires (except at a limited potential region for the CBD sensitized nanoparticles), consistently with the much lower surface area. The effect of the QDs deposition method was also evaluated and the higher photocurrents obtained with CBD were correlated to increased recombination resistances. The device also showed to be stable over more than 30 min operation with a photocurrent loss lower than 10% for NPs electrodes and 15% for HNWs electrodes. The present study may pave the way toward nanoscale heterostructures for H$_2$ generation systems, encompassing the synergistic combination of quantum dot absorbers with different strategies for ortogonalization of light harvesting and carrier collection.

4. Experimental Section

Synthesis of Vertically Aligned TiO_2 Hollow Nanowire (HNWs) Array: Vertically aligned TiO_2 hollow nanowires onto FTO substrates were grown in two stages. In the first step, a 200 nm-thick ZnO film as a seed layer was deposited on the FTO substrate using radio frequency magnetron sputtering. Further, the ZnO seed layer coated FTO substrate was immersed into aqueous solution containing 0.025 M zinc nitrate hexahydrate and 0.025 M hexamethylentetramine. Subsequently, the sample was kept at 85 °C for 10 h for the growth of vertically aligned ZnO nanorods array (NR). After ZnO NR growth, the substrates were taken out of the bath, rinsed with deionized water. In the second stage, ZnO NRs were utilized as a template for TiO_2 layer growth. The resultant ZnO NR array template was transferred to aqueous solution consisting of 0.075 M ammonium hexafluorotitanate and 0.2 M boric acid for TiO_2 layer deposition. Subsequently the TiO_2 layer coated ZnO NRs were immersed in a 0.5 M boric acid solution for 1 h to remove the ZnO NR template and rinsed with DI water. Finally, vertically aligned TiO_2 HNWs arrays are obtained. The HNWs samples were calcined at 500 °C for 0.5 h under Ar atmosphere to improve its crystallinity. The thickness of the electrodes was ~5 μm, as measured by cross-sectional scanning electron microscopy (see Supporting Information, Figure SI1).

Preparation of TiO_2 Nanoparticulated Electrode: Commercial titania paste (Solaronix DSL 18NR, Switzerland, 20 nm particle size) was coated on FTO (SnO$_2$:F, TEC 15) substrate by doctor blade technique and then dried at 80 °C. Prior to TiO_2 nanoparticle deposition, the FTO substrates were covered by a compact layer of TiO_2 deposited by spray pyrolisis of titanium(IV)bis(acetoacetonato) di(isopropanoxylate). These electrodes were subsequently sintered at 450 °C for 30 min. The thickness of the electrodes was ~4 μm (see Supporting Information, Figure SI1).

QDs-Sensitization Onto TiO_2: In order to investigate the influence of QDs coverage on mesoporous TiO_2 two different QDs assembling methods namely (a) chemical bath deposition (CBD) and (b) successive ionic layer adsorption and reaction (SILAR) were adopted for CdSe. A CdS seed layer was preliminarily coated only for the CBD electrodes. Briefly, 3 coating cycles of CdS were applied on the TiO_2 surface which acted as seed layer for CdSe deposition on TiO_2 surface. By the assisted CBD method, CdSe QDs were assembled on TiO_2 surface in a chemical bath containing the mixture of 80 mM CdSO$_4$ and 80 mM sodium selenosulphate (Na$_2$SeSO$_3$) solution with 120 mM nitriloacetic acid. The electrodes were immersed in the chemical bath at 10 °C for 12 h in the dark. Finally the films were taken out from the bath, rinsed with deionized water and dried with nitrogen. CdSe QDs were also deposited by SILAR onto both TiO_2 structures. The electrodes were successively immersed in two different ethanolic solutions for 1 min each, consisting of 0.03 M Cd(NO$_3$)$_2$, and 0.03 M Se^{2-} respectively. This method was developed by the Grätzel's group.[31] The electrodes were alternatively dipped in these solutions inside a glovebox under N$_2$ atmosphere. Following each immersion, rinsing and drying was undertaken using pure ethanol and a

www.MaterialsViews.com

ADVANCED
ENERGY
MATERIALS
www.advenergymat.de

FULL PAPER

N_2 gun, respectively. All these processes constitute one SILAR cycle and a total of 7 cycles were carried out. All the samples analyzed in this study have been coated with a ZnS coating, after CdSe sensitization, by twice dipping alternately into 0.1 M $Zn(CH_3COO)_2$ and 0.1 M Na_2S solutions for 1 min/dip, rinsing with Milli-Q ultrapure water between dips.[32]

Structural, Optical and Electrochemical Characterization: Structural inspection of the samples was carried out using a JEOL JEM-3100F field emission scanning electron microscope (SEM) and a JEOL JSM 7600F field emission transmission electron microscope (TEM). The surface area of the TiO_2 nanoparticulated structures was measured by gas adsorption measurements, BET, performed on a Micromeritics ASAP 2020 surface area and porosity analyzer with the ASAP 2020 V3.04 E software. The surface area and porosity of the TiO_2 hollow nanowires was theoretically calculated based on electron microscope images. (See Supporting information, Figure SI2). The transmittance and diffuse reflectance spectra of the photoelectrodes were recorded between 300 and 800 nm by a Cary 500 UV-VIS Varian photospectroscometer. An integrating sphere was used for the diffuse reflectance measurements. The absorbance was calculated as:

$$A = -\log(T + R) \tag{1}$$

Steady state and chopped light current density voltage (j-V), Electrochemical Impedance Spectroscopy (EIS) and V_{oc} decay measurements were carried out using a FRA equipped PGSTAT-30 from Autolab. A three-electrode configuration was used, where the TiO_2/CdS/CdSe photo-electrode was connected to the working electrode, a Pt wire was connected to the counterelectrode and a saturated Ag/AgCl was used as the reference electrode. An aqueous solution containing 0.25 M Na_2S and 0.35 M Na_2SO_3 as sacrificial hole scavenger was used as the electrolyte to prevent photocorrosion of the QDs. Nitrogen was bubbled during 30min before testing to avoid the presence of oxygen (electron acceptor) in the solution. The pH of the solution was 12.8 and all the electrochemical measurements were referred to the reversible hydrogen electrode (RHE) by the equation $V_{RHE} = V_{Ag/AgCl} + 0.197 + pH(0.059)$. The electrodes were illuminated using a 35W Xe lamp, with a 380 nm cutoff filter. The light intensity was adjusted with a thermopile to 100 mW/cm^2, with illumination through the substrate. Additionally, a two electrode configuration was used, with testing parameters identical to those described above, and removing the reference electrode. EIS measurements were carried out in a three electrode configuration, applying 20 mV AC signal and scanning in a frequency range between 400 KHz and 0.1 Hz, at different applied biases. V_{oc} decay measurements were carried out by measuring upon switching off the light source. Labeling experiments of the evolved gases were carried out using gas chromatography mass spectroscopy GC/MS. A quadrupole Pfeiffer Vacuum model Thermostar GSD301T with a mass interval ranging down to 300 uma was used. The evolved gas was collected from the electrochemical cell in an inverted burette and extracted with a gas-tight syringe provided with an exit valve.

Supporting Information

Supporting Information is available from the Wiley Online Library or from the author.

Acknowledgements

[1] M. G. Walter, E. L. Warren, J. R. McKone, S. W. Boettcher, Q. X. Mi, E. A. Santori, N. S. Lewis, *Chem. Rev.* **2010**, *110*, 6446.
[2] A. Fujishima, K. Honda, *Nature* **1972**, *238*, 37.
[3] X. B. Chen, S. H. Shen, L. J. Guo, S. S. Mao, *Chem. Rev.* **2010**, *110*, 6503.
[4] M. A. Holmes, T. K. Townsend, F. E. Osterloh, *Chem. Commun.* **2012**, *48*, 371.
[5] S. Y. Yang, D. Prendergast, J. B. Neaton, *Nano Lett.* **2012**, *12*, 383.
[6] I. Thomann, B. A. Pinaud, Z. B. Chen, B. M. Clemens, T. F. Jaramillo, M. L. Brongersma, *Nano Lett.* **2011**, *11*, 3440.
[7] E. Thimsen, F. Le Formal, M. Gratzel, S. C. Warren, *Nano Lett.* **2011**, *11*, 35.
[8] N. Chouhan, C. L. Yeh, S. F. Hu, J. H. Huang, C. W. Tsai, R. S. Liu, W. S. Chang, K. H. Chen, *J. Electrochem. Soc.* **2010**, *157*, B1430.
[9] J. Hensel, G. M. Wang, Y. Li, J. Z. Zhang, *Nano Lett.* **2010**, *10*, 478.
[10] H. Kim, M. Seol, J. Lee, K. Yong, *J. Phys. Chem. C* **2011**, *115*, 25429.
[11] H. Kim, M. Seol, J. Lee, K. Yong, *J. Phys. Chem. C* **2011**, *115*, 25429
[12] H. M. Chen, C. K. Chen, Y. C. Chang, C. W. Tsai, R. S. Liu, S. F. Hu, W. S. Chang, K. H. Chen, *Angew. Chem. Int. Ed.* **2010**, *49*, 5966.
[13] R. Tena-Zaera, J. Elias, C. Levy-Clement, *Appl. Phys. Lett.* **2008**, *93*.
[14] N. Guijarro, Q. Shen, S. Gimenez, I. Mora-Sero, J. Bisquert, T. Lana-Villarreal, T. Toyoda, R. Gomez, *J. Phys. Chem. C* **2010**, *114*, 22352.
[15] E. S. Smotkin, S. Cerveramarch, A. J. Bard, A. Campion, M. A. Fox, T. Mallouk, S. E. Webber, J. M. White, *J. Phys. Chem.* **1987**, *91*, 6.
[16] S. Gimenez, T. Lana-Villarreal, R. Gomez, S. Agouram, V. Munoz-Sanjose, I. Mora-Sero, *J. Appl. Phys.* **2010**, *108*.
[17] M. Samadpour, S. Giménez, P. P. Boix, Q. Shen, M. E. Calvo, N. Taghavinia, A. Iraji zad, T. Toyoda, H. Míguez, I. Mora-Seró, *Electrochim. Acta* **2012**, *75*, 139.
[18] H. Dotan, K. Sivula, M. Gratzel, A. Rothschild, S. C. Warren, *Energy Environ. Sci.* **2011**, *4*, 958.
[19] B. M. Klahr, T. W. Hamann, *J. Phys. Chem. C* **2011**, *115*, 8393.
[20] B. M. Klahr, S. Gimenez, F. Fabregat-Santiago, J. Bisquert, T. W. Hamann, *Energy Environ. Sci.* **2012**, *5*, 7626.
[21] I. Mora-Sero, S. Gimenez, F. Fabregat-Santiago, R. Gomez, Q. Shen, T. Toyoda, J. Bisquert, *Acc. Chem. Res.* **2009**, *42*, 1848.
[22] V. Gonzalez-Pedro, X. Q. Xu, I. Mora-Sero, J. Bisquert, *Acs Nano* **2010**, *4*, 5783.
[23] J. Bisquert, *J. Phys. Chem. B* **2002**, *106*, 325.
[24] J. Bisquert, D. Cahen, G. Hodes, S. Ruhle, A. Zaban, *J. Phys. Chem. B* **2004**, *108*, 8106.
[25] F. Fabregat-Santiago, G. Garcia-Belmonte, I. Mora-Sero, J. Bisquert, *Phys. Chem. Chem. Phys.* **2011**, *13*, 9083.
[26] I. Robel, V. Subramanian, M. Kuno, P. V. Kamat, *J. Am. Chem. Soc.* **2006**, *128*, 2385.
[27] S. Gimenez, H. Dunn, P. Rodenas, F. Fabregat-Santiago, S. Miralles, E. Barea, R. Trevisan, A. Guerrero, J. Bisquert, *J. Electroanal. Chem.* **2012**, *668*, 119.
[28] J. Bisquert, F. Fabregat-Santiago, I. Mora-Sero, G. Garcia-Belmonte, S. Gimenez, *J. Phys. Chem. C* **2009**, *113*, 17278.
[29] J. Bisquert, A. Zaban, M. Greenshtein, I. Mora-Sero, *J. Am. Chem. Soc.* **2004**, *126*, 13550.
[30] A. Zaban, M. Greenshtein, J. Bisquert, *ChemPhyschem* **2003**, *4*, 859.
[31] H. Lee, M. K. Wang, P. Chen, D. R. Gamelin, S. M. Zakeeruddin, M. Gratzel, M. K. Nazeeruddin, *Nano Lett.* **2009**, *9*, 4221.
[32] Q. Shen, J. Kobayashi, L. J. Diguna, T. Toyoda, *J. Appl. Phys.* **2008**, *103*.